Available online at www.sciencedirect.com
SCIENCE DIRECT®
Advances in Space Research 36 (2005) 1909–1915
ADVANCES IN SPACE RESEARCH (a COSPAR publication)
www.elsevier.com/locate/asr

What is Cluster telling us about magnetotail dynamics?

Wolfgang Baumjohann *, Rumi Nakamura

Institut für Weltraumforschung, Österreichische Akademie der Wissenschaften, Schmiedlstr. 6, 8042 Graz, Austria

Received 30 October 2002; received in revised form 5 February 2004; accepted 8 February 2004

Abstract

In this review, we report on some new aspects of magnetotail dynamics found in the data of the first traversal of the magnetotail by the Cluster quartet in summer and autumn 2001: (1) The electron drift instrument made the first direct measurements of tail lobe convection. The statistical data shows convection toward the center of the plasma sheet, with a clear dependence on the sign of the interplanetary magnetic field B_Z component. Moreover, a dawn–dusk shear (if one compares convection in opposite lobes) for B_Y-dominated interplanetary field hints to an interconnection of open lobe field lines with the interplanetary medium. (2) At times the tail current sheet resembles a one-dimensional Harris sheet, which might get as thin as 500 km and may carry current densities as high as 20–40 nA/m^2. (3) At other times, the current sheet may exhibit rapid kink-type flapping motion with vertical velocities of 50–100 km/s. During these intervals the current sheet clearly exhibits a bifurcated structure, with two current density maxima around a region of much reduced current in the center of the plasma sheet.

Keywords: Cluster; Magnetotail dynamics; Magnetosphere; Current sheet

1. Introduction

The Cluster quartet of satellites allows, for the first time, to separate spatial and temporal variations in arbitrary geometry measurements of space plasma parameters. This is of particular importance in a highly variable and dynamic region like the Earth's magnetotail and provides completely new insight into magnetotail dynamics. Further, new understanding comes from new and improved instrumentation.

The Cluster spacecraft were launched in summer 2000 and put into a polar orbit. They became operational since February 2001, after five months' commissioning phase, and they experienced the first tail passage from July to October 2001. The four satellites had separations ranging from 1500 to 3000 km in the magnetotail region during this period. The orbit of the Cluster quartet is almost fixed in the inertial frame, so that they pass the magnetotail from the dawn side flank to the dusk side flank as the Earth's magnetosphere revolves around the Earth once in a year in the inertial frame centered in the Earth.

Of particular interest is the orientation and shape of the Cluster tetrahedron when it traverses the plasma sheet at its apogee from north to south at a radial distance of about $20R_E$. Fig. 1 shows the typical tetrahedron configuration during current sheet traversals: of particular importance for the current sheet studies will be that spacecraft (s/c) 3 leads the other s/c by about 1500 km on their north-to-south orbit. The east–west and Sun–Earth pairs have been used in other studies (e.g., Nakamura et al., 2002a; Zhang et al., 2002; Petrukovich et al., 2003) not discussed here.

The Cluster data presented in this review stem from three instruments: (1) the Flux-Gate Magnetometer (FGM; Balogh et al., 2001); (2) the Cluster Ion Spectrometry (CIS; Rème et al., 2001) experiment; and (3) the Electron Drift Instrument (EDI; Paschmann et al.,

* Corresponding author. Tel.: +43 316 4120 501; fax: +43 316 4120 590.
E-mail address: baumjohann@oeaw.ac.at (W. Baumjohann).

0273-1177/$30
doi:10.1016/j.asr.2004.02.021

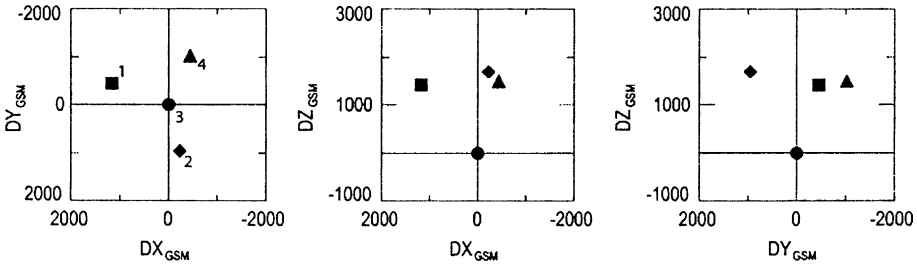

Fig. 1. Typical orientation of the Cluster tetrahedron (s/c 1–4) during plasma sheet traversals in 2001.

2001). EDI is a novel instrument that observes the electric field by measuring the drift velocity of artificially emitted electron beams in the plane perpendicular to the local magnetic field. By using this technique, the drift velocity is measured successfully even in the more tenuous regions of the magnetosphere like the near-Earth tail lobes.

2. Tail lobe convection

The interplanetary magnetic field (IMF) interacts with the Earth's dayside magnetic field through magnetic reconnection. The solar wind drags the reconnected field lines from the dayside to the nightside, stretches the field lines, and stores the energy in the form of magnetic tension. The stored energy is released when the open magnetic field lines reconnect again to form closed field lines, which return toward the Earth. The convection in the lobe is tightly connected to dayside reconnection. The plasma density in the near-Earth lobe is typically lower than 0.01/cc, which makes the observations of lobe convection by particle detectors difficult. Here, we will show observations of the averaged near-Earth tail lobe convection and its relationship to IMF polarity by using the Electron Drift Instrument (EDI) aboard the Cluster spacecraft.

Noda et al. (2003) averaged spin resolution data (4-s values) to a 5-min data set for the comparison with ACE solar wind data. They used EDI data from July to October 2001 from three Cluster spacecraft (on s/c 4 EDI is not operated) within $-15 \leqslant X_{\mathrm{GSM}} \leqslant -5R_E$, $|Y_{\mathrm{GSM}}| \leqslant 12R_E$, $4 \leqslant |Z_{\mathrm{GSM}}| \leqslant 12R_E$. The criterion for Y_{GSM} serves to exclude the low latitude boundary layer. The criterion for Z_{GSM} was chosen to avoid the plasma sheet. They then divided the data into four categories based on 90° IMF clock angle sectors centered on $\pm B_Z$ and $\pm B_Y$. For the IMF, they used the ACE magnetic field data, first shifting the time tags of the magnetic field data by using ACE solar wind velocity data (so that the observation position corresponds to $X = 0$). The EDI data for the four IMF states were then averaged into four different bins. Fig. 2 shows the most prominent features found.

We can draw the following conclusions from this figure. First, the vectors point toward the neutral sheet in both panels. Second, the flow direction in the Y–Z plane (right-hand panel) changes between $+B_Y$ and $-B_Y$ conditions. For $+B_Y$, the vectors in all four quadrants have a counterclockwise component in this Y–Z plane, while for $-B_Y$ a clockwise component appears (that the vector in the northern dawn quadrant in the $-B_Y$ case has a different sense may be caused by the small amount of data for that state/bin). Third, as expected, the velocity becomes larger for IMF $-B_Z$ because for this IMF polarity dayside reconnection occurs most efficiently.

The most notable point is the difference of the velocity in the Y–Z plane under $\pm B_Y$ conditions. For $+B_Y$,

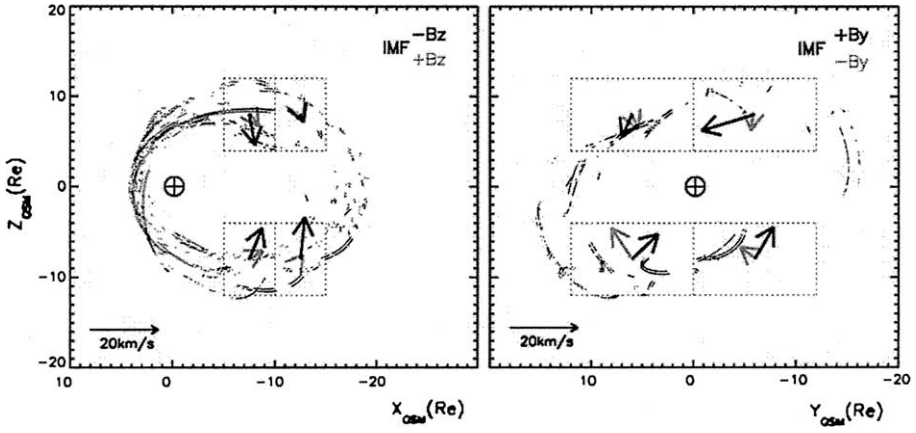

Fig. 2. Average lobe convection for different IMF clock angles (after Noda et al., 2003).

field lines, which reconnect with the geomagnetic field in the dayside region and are subsequently transported to the nightside by the solar wind, have a duskward velocity component in the northern and a dawnward component in the southern lobe. This will make a counterclockwise rotation of the convection in the nightside. The opposite is true for $-B_Y$. In terms of electric field, clockwise and counterclockwise rotation of the flow for $-B_Y$ and $+B_Y$ conditions correspond to $-E_Z$ and $+E_Z$, respectively.

3. Current sheet thinning

Nakamura et al. (2002b) reported Cluster observations of a fast flow event in the plasma sheet associated with a small substorm intensification at 1838 UT on 12 August 2001. Cluster, located in the plasma sheet, experienced significant thinning of the current sheet associated with a high-speed Earthward flow of 900 km/s. The authors found that the disturbances in the B_X and B_Y components were well correlated and therefore transformed the data into a minimum variance coordinate system. Fig. 3 shows the proton velocity from s/c 1, 3, and 4 (the ion spectrometer does not work on s/c 2) and the magnetic field data from the four spacecraft in this coordinate system, with X', Y', and Z' as the maximum, intermediate, and minimum variance direction (see also insert in Fig. 3). It can be seen that high-speed flow as well as field perturbation occur mainly in the X' direction.

The flow and field disturbance can be divided into three intervals, delineated by the clashed lines. (1) During the first interval, when the flow starts to develop, the field traces for each s/c are quite different and so are the flow traces. The flow at s/c 3 is more developed compared to that at s/c 1 or 4. Since s/c 3 was located southward and closer to the central plasma sheet, the difference suggests that the flow is more developed near the neutral sheet. (2) During the second interval, on the other hand, the three traces of the flows are more similar, although the satellites are located at quite different places relative to the neutral sheet, i.e., north and south of the neutral sheet. Hence, high-speed flow seems spread throughout the plasma sheet. (3) During the third interval, the three satellites in the northern hemisphere, which are located nearly at the same distance from the neutral sheet, differed significantly in the magnetic field traces. This indicates an enhancement in the local current density at the three northern spacecraft regions. On the other hand, the flow traces are similar to that of interval (2).

Since the magnetic field perturbation is predominantly in the X' direction and the flow profile was similar among the satellites, the data was fitted to the Harris current sheet to examine quantitatively how the current

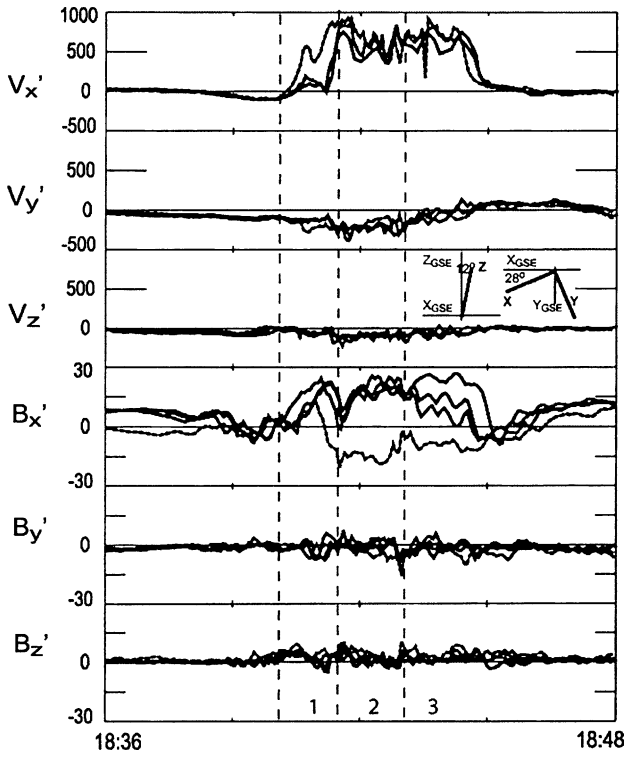

Fig. 3. Magnetic field and ion velocity in MVA coordinates (from Nakamura et al., 2002b). The data from the southernmost s/c 3 are shown as dashed traces. The insert gives the MVA coordinates.

sheet is structured during the flow interval. In a Harris sheet the magnetic field is represented by $B_X(z) = B_L \tanh\{(z - z_0)/L\}$, where B_L is the lobe field outside the current sheet, z_0 is the location of the neutral sheet and L is the half-thickness of the current sheet. Simultaneous measurements from three spacecraft allow to estimate the three parameters and to compare the estimated model B_X at the location of the fourth spacecraft with the actual data to check the validity of the estimation. The model estimates are accepted whenever the difference between model and data does not exceed a factor of 2 and $15 < B_L < 35$ nT (the latter condition is important to ensure that the model covers a major part of the current sheet up to lobe field, which is expected to be 25–30 nT based on the previous lobe field values). Various combinations of the three spacecraft were used, but always included the most southern s/c 3, in the model.

Fig. 4 shows the result of the Harris sheet estimation for several sequences before and during the flow interval together with the most relevant data traces. Results shown are mostly concentrated during interval (2). Nonetheless, it can be seen how the current sheet structure changes during the flow event. Before the onset of the flow, the spatial scale of the current sheet is 5000 km. After southward excursion of the current

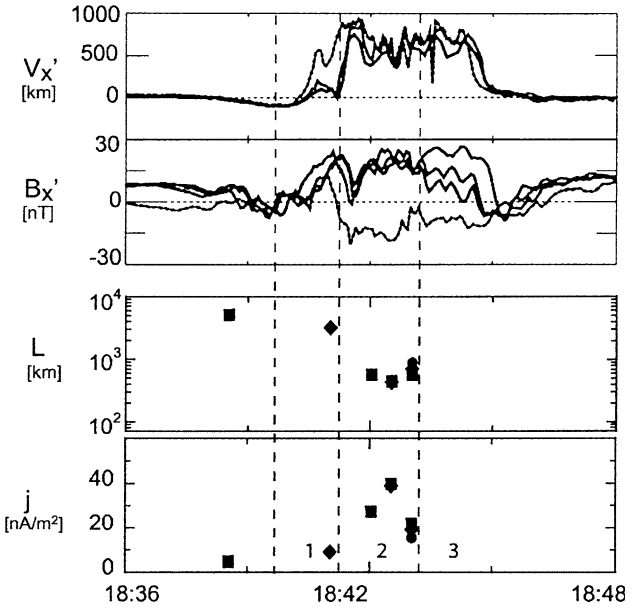

Fig. 4. Sunward component of ion velocity and magnetic field (data) and current sheet half width and current density (model). The data from the southernmost s/c 3 are again shown as dashed traces (after Nakamura et al., 2002b).

sheet, during interval (2), the scale reduces to 500 km, which is comparable to the ion inertial length. The maximum current density predicted from the Harris sheet model increases from 5–10 to 20–40 nA/m^2.

4. Bifurcated current sheets

The 1500 km separation of the Cluster spacecraft during the 2001 tail passages was not well suited to study the internal structure of the current sheet. However, at times, the current sheet underwent large-scale flapping motions with north–south velocities of up to 100 km/s. Since the current density profile did not change during these up-and-down motions, comparison of the difference in the magnetic fields measured by the southernmost and the northern spacecraft triad allowed the determination of the current density profile. On two different days, the tail current sheet clearly did not resemble a Harris sheet, but rather exhibited a double-peaked, bifurcated structure, with a pair of current sheets separated by a layer of weak quasi-uniform magnetic field in the center of the plasma sheet. This bifurcated structure seen around $20R_E$ down tail is very similar to that found by Hoshino et al. (1996) in the distant magnetotail, around $100R_E$.

Runov et al. (2003) examined the current sheet structure and motion at $X_{GSM} = -19.5R_E$ on 29 August 2001, during the recovery phase of an isolated substorm. Starting at 1055:30 UT, Cluster detects a sudden expansion or flapping motion of the current sheet: a significant difference between B_X measured by s/c 3 (the southernmost one) and B_X measured by the other three spacecraft, and rapid variations of the magnetic field appear (see Fig. 5). Between 1055 and 1102 UT a set of short depressions of B_X with a characteristic time scale of 70–90 s occurs. The interval 1103–1107 corresponds to a gradual crossing of the neutral sheet: Cluster travels from the northern ($B_X > 0$) into the southern hemisphere ($B_X < 0$). During 1059:30–1102:00 UT, s/c 3 stays in a region of very weak ($-0.5 < B_X < 2$ nT) magnetic field, while the magnetic field measured by the other three spacecraft continues to vary in the range 0–8 nT. At about 1100:10 and at about 1101:40 UT all four spacecraft detect the same very weak magnetic field; at 1101:40 UT all three magnetic field components at all four Cluster spacecraft are close to zero.

Runov et al. (2003) shows that the variations of B_X are caused by a wave-like transient passing the Cluster tetrahedron. A multi-point timing analysis yields that the wave propagates toward dusk with a velocity of

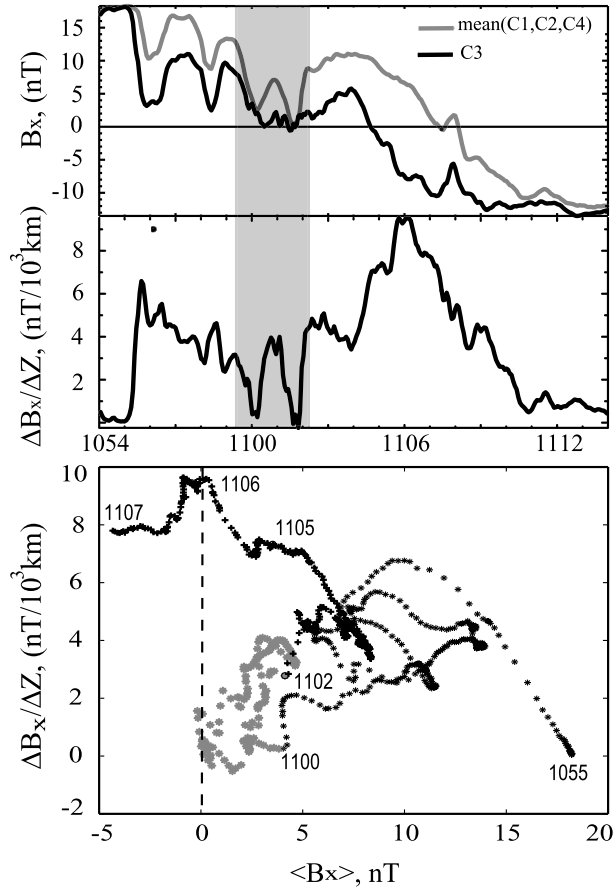

Fig. 5. Current sheet structure during 1055–1107 UT. Upper panel: mean B_X from s/c 1, 2, and 4 (gray curve) and B_X from s/c 3 (black curve). Middle panel: vertical gradient of the magnetic field. Bottom panel: magnetic field gradient versus average B_X, asterisks correspond to 1055–1100 UT, gray bullets to 1100–1102 UT, and crosses to 1102–1107 UT (from Runov et al., 2003).

about 200 km/s and has a characteristic period near 90 s. The average normal (north–south) velocity of the current sheet motion is 60 km/s. The wavelength of the transient wave is about of $3R_E$, and the amplitude near $0.5R_E$. Consequently, the wave profile is not very steep and the assumption of flat current sheet geometry is still valid.

Since s/c 1, 2, and 4, which are located in a plane approximately parallel to the $Z_{GSM} = 0$ plane and form a triangle with a characteristic scale of ~1700 km, detect nearly identical B_X, one can assume that the current sheet is parallel to equatorial plane within the scale of interspacecraft separation. Hence, the difference between the mean value of $\langle B_X \rangle$ measured by s/c 1, 2, and 4, and B_X from s/c 3 is a measure of the vertical (north–south) gradient of the magnetic field in the current sheet. At 1055:30 UT Cluster detects a sudden jump of the vertical magnetic field gradient from zero up to 6 nT/1000 km, then a gradual decrease down to approximately 3 nT/10^3 km at 1059:30 UT, a sudden decrease down to zero at 1100:10 UT, followed by an increase up to 4 nT/10^3 km, a drop to zero at 1101:40 UT, and then a jump to 5 nT/10^3 km at 1102:00 UT. After 1102 UT the vertical gradient of B_X changes smoothly and looks symmetric at 1106 UT, when $\langle B_X \rangle = 0$. The maximum gradient is about 9 nT/10^3 km.

As may be seen from the ΔB_X versus $\langle B_X \rangle$ diagram shown in the bottom panel of Fig. 5, the current sheet geometry before 1102 UT and after 1103 UT significantly differs. Before 1102 UT local maxima of the magnetic field gradient are located not in the vicinity of zero magnetic field, as one may expect from the Harris model, but around a magnitude field of 5–10 nT, which is about half the lobe field, B_L. Furthermore, contrary to the Harris-type sheet, during this interval the magnetic field gradient is zero at $\langle B_X \rangle = 0$. Expecting a current density distribution nearly symmetrical with respect to $\langle B_X \rangle = 0$, the current sheet must have a bifurcated structure during this interval. After 1103 UT the maximum value of the magnetic gradient (current density) occurs in the vicinity of zero magnetic field, which is normal for Harris-type current sheet configuration.

The observation of current sheet bifurcation is supported by a detailed analysis of the interval around 1101 UT (shaded gray in Fig. 5 and upper panel of Fig. 6). At 1100:10 UT all four spacecraft measure the same weak (about 2.5 nT) magnetic field. The same situation holds at 1101:40 UT; all four Cluster spacecraft observe a very weak (about 0.5 nT) magnetic field. Therefore, at 1100:10 UT and at 1101:40 UT Cluster is located in an extended layer of very weak uniform magnetic field in the vicinity of the neutral sheet. Between 1100:10 UT and 1101:40 UT the traces of s/c 3 and the northern group (s/c 1, 2, and 4) are different: s/c 3 stays in a weak field region (about 1 nT), while the northern group measures 6–8 nT. The average vertical gradient of the magnetic field within the northern group of spacecraft is 9 nT/10^3 km, which corresponds to a current density of 7 nA/m^2.

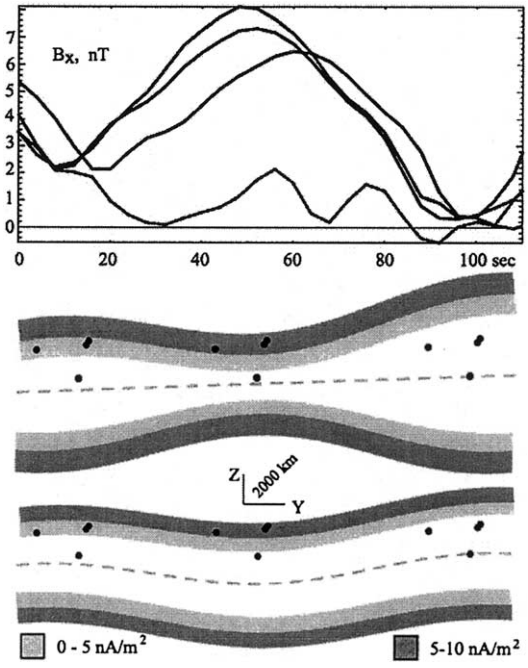

Fig. 6. A possible interpretation of the Cluster/FGM measurements around 1101 UT (upper panel): current sheet bifurcation associated with a sausage-type or a kink-type flapping oscillation (lower panels; after Runov et al., 2003).

The lower panels of Fig. 6 illustrate the bifurcated current sheet model, describing this situation. The two panels illustrate two possible configurations of the currents in the bifurcated current sheet during the interval 1100:10–1101:40 UT; an expansion–contraction wave (sausage mode) and a wavy flapping motion (kink mode). For the sausage mode the thickness of the current sheet varies along the cross-tail direction, so a set of magnetic holes may appears, for the kink mode the current sheet forms a wave structure, while its thickness remains relatively constant. The characteristic scale of the weak uniform field layer is of the order of the separation between the spacecraft, 2000 km.

While Runov et al. (2003) were unable to distinguish between sausage and kink mode, since the Cluster quartet did not cross the neutral sheet during their observations of the flapping motion, Sergeev et al. (2003) found a different event, observed on 26 September 2001, with full traversals and could identify the kink mode. Fig. 7 displays the detailed view of observations during three oscillations which have an apparent period about 3 min. To analyze the flapping oscillation in more detail they used inter-s/c timing as well as Minimum Variance Analysis. All but one MVA determinations gave well resolved MVA normals (with the intermediate-to-minimal

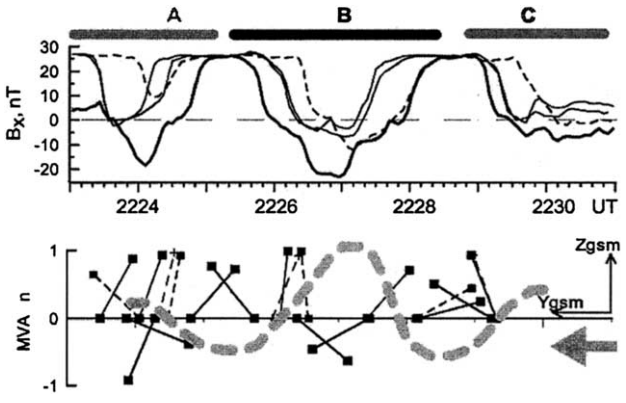

Fig. 7. Observations during three complete flapping oscillations: variations of B_X-components at four s/c and Y–Z projection of current sheet normals determined from minimum variance during upward and downward phases of flapping (those from s/c 3 are marked by solid squares). A sketch of the expected flapping wave is shown by the thick dashed line (after Sergeev et al., 2003).

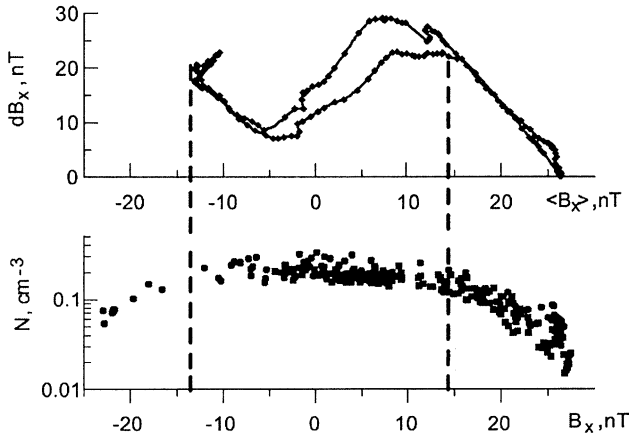

Fig. 8. Distribution of ion density during all three oscillations and magnetic field difference for oscillation B versus B_X (after Sergeev et al., 2003).

eigenvalue ratio exceeding 3). Their projections to the Y–Z plane are displayed in the lower panel of Fig. 7; the X-component of the normal is always smallest, so the tilt in X–Z plane is insignificant. The wave travels again toward dusk, but in this case has a larger amplitude, near $1R_E$.

Complete coverage and most consistent results come from data of s/c 3, which crossed the entire sheet between the two lobes: the same sense of sheet tilt in northern and southern regions implies that the sheet is tilted as a whole (suggesting the kink wave mode) rather than being locally expanded and contracted (like in the sausage mode). Other s/c show typically smaller slopes of the normal (probing the smaller part, near the tops of oscillations), in many cases their average (except for upward phases of oscillations A and B) are of the same sense and agree with s/c 3.

Using the difference $\Delta B_X = B_{X1} - B_{X3}$ of the X-components measured by s/c 1 and 3 and the s/c separation ΔZ yields the current density $\Delta B_X/\mu_0 \Delta Z_{\cos}\Phi$, where Φ is the angle between Z axis and tilted current sheet normal. As a label of position in the current sheet where this current density has to be assigned, the B_X component value in the mid point, that is $\langle B_X\rangle = 0.5(B_{X3} + B_{X1})$, is used. A hodogram (at the top of Fig. 8) of ΔB_X versus $\langle B_X\rangle$ during the most deep plasma sheet crossing (oscillation B, after 2225:20 UT) display a systematic behavior, with a deep local minimum in the central part (where $B_X \sim 0$) and the maximum ΔB_X at $|B_X| \sim 10$–15 nT. This bifurcated current structure was nearly stable for the next 15 min. The ΔB_X value at the current maximum of about 25 nT yields $\sim$12 nA/m^2 (vertical separation abut 1500 km), which is the lower limit for the current density in the maximum region. The bifurcated current peaks at $|B_X| \sim 0.5B_L$ (lobe field $B_L \sim 27$ nT) and has a deep (a factor 2–3 lower than the peak value) broad valley in the central part of the current sheet. Note that the plasma density shows the typical flat profile between $\pm 0.5B_L$, and then drops off toward the lobe.

Hoshino et al. (1996) suggest that the double-peaked current sheet structure is the consequence of magnetic reconnection. The reconnection process includes the formation of an X-type magnetic configuration and significant plasma acceleration along the sheet. However, neither of the Runov et al. nor the Sergeev et al. case showed any signatures of a relationship to reconnection (dipolarization or fast flows). Another possible mechanism leading to current sheet bifurcation was introduced by Zelenyi et al. (2002). Their analysis indicates that bifurcation is a typical process during the evolution or aging of a current sheet. Since the present experimental data are insufficient to distinguish between these two candidate processes (or give hints to yet another one), the process leading to a bifurcated current sheet formation remains an open question. We will most likely have to wait for Cluster tail passages with smaller separation. Separations of some hundred kilometers are planned for the 2003 tail season.

Acknowledgments

The data and analysis presented in this review would not exist without the help of many individuals. In particular, we thank H. Noda, A. Runov, V.A. Sergeev, M. Volwerk, and T.L. Zhang who collaborated with us or led the different studies described here. We are also grateful to A. Balogh, K.-H. Glaßmeier, B. Klecker, G. Paschmann, J. Quinn, H. Rème, and their teams, who were instrumental in building and operating the three Cluster instruments used in our studies and kindly allowed us to use their data.

References

Balogh, A., Carr, C.M., Acuña, M.H., et al. The Cluster magnetic field investigation: overview of in-flight performance and initial results. Ann. Geophys. 19, 1207–1217, 2001.

Hoshino, M., Nishida, A., Mukai, T., Saito, Y., Yamamoto, T. Structure of plasma sheet in magnetotail: double-peaked electric current sheet. J. Geophys. Res. 101, 24,775–24,786, 1996.

Nakamura, R., Baumjohann, W., Klecker, B., et al. Motion of the dipolarization front during a flow burst event observed by Cluster. Geophys. Res. Lett. 29, 1942, 2002a.

Nakamura, R., Baumjohann, W., Runov, A., et al. Fast flow during current sheet thinning. Geophys. Res. Lett. 29, 2140, 2002b.

Noda, H., Baumjohann, W., Nakamura, R., et al. Tail lobe convection observed by Cluster/EDI. J. Geophys. Res. 108, 1288, 2003.

Paschmann, G., Quinn, J.M., Torbert, R.B., et al. The Electron Drift Instrument on Cluster: overview of first results. Ann. Geophys. 19, 1273–1288, 2001.

Petrukovich, A.A., Baumjohann, W., Nakamura, R. Plasma sheet structure during strong northward IMF. J. Geophys. Res. 108, 1258, 2003.

Rème, H., Aostin, C., Bosqued, J.M., et al. First multispacecraft ion measurements in and near the Earth's magnetosphere with the identical Cluster ion spectrometry (CIS) experiment. Ann. Geophys. 19, 1303–1354, 2001.

Runov, A., Nakamura, R., Baumjohann, W., Zhang, T.L., Volwerk, M., Eichelberger, H.-U., Balogh, A. Cluster observation of a bifurcated current sheet. Geophys. Res. Lett. 30, 1036, 2003.

Sergeev, V., Runov, A., Baumjohann, W., et al. Current sheet flapping motion and structure observed by Cluster. J. Geophys. Res. 30, 1327, 2003.

Zelenyi, L., Delcourt, D.C., Malova, H.V., Sharma, A.S. "Aging" of the magnetotail current sheets. Geophys. Res. Lett., 29, 2002.

Zhang, T.L., Baumjohann, W., Nakamura, R., Balogh, A., Glaßmeier, K.-H. A wavy twisted neutral sheet observed by Cluster. Geophys. Res. Lett. 29, 1899, 2002.